THE JOURNAL OF PHYSICAL CHEMISTRY B

Article

pubs.acs.org/JPCB

An Active Site Water Broadens Substrate Specificity in *S*-Ribosylhomocysteinase (LuxS): A Docking, MD, and QM/MM Study

WenJuan Huang, Rami Gherib, and James W. Gauld*

Department of Chemistry and Biochemistry, University of Windsor, Windsor, Ontario N9B 3P4, Canada

Supporting Information

ABSTRACT: Type-2 quorum sensing (QS-2) is a cell−cell signaling process known to be used by a number of pathogenic bacteria and to play important roles in their population growth and virulence. *S*-ribosyl homocysteinase (LuxS) is a key enzyme in the formation of the signaling molecule of QS-2, autoinducer II (AI-2). In this study, substrate (*S*-ribosylhomocysteine: SRH) binding and possible initial reaction steps of its catalytic mechanism leading to formation of a putative 2-keto-SRH intermediate have been examined. Specifically, docking and MD simulations were used to gain insights into the structure of the active-site-bound substrate complex. An ONIOM QM/MM hybrid method was then used to elucidate the mechanism of the first stage of the enzyme catalytic process. It is shown that the substrate may bind within the active site when its ribosyl moiety is in the α- (α-SRH) or β-furanose (β-SRH) configuration or as a linear aldose (linear-SRH). The α-SRH complex is preferred, lying 47.5 kJ mol^{-1} lower in energy than the next lowest energy initial complex β-SRH. However, the MD and QM/MM calculations indicate that an active site water stably locates within the active site and that it can facilitate ring-opening of either α-SRH or β-furanose, leading to formation of a common active-site-bound 2-keto-SRH intermediate, without the need to pass through a linear aldose SRH configuration. Hence, regardless of the ribose's configuration within the bound SRH substrate, LuxS is able to catalyze the conversion of SRH to a common 2-keto-SRH intermediate.

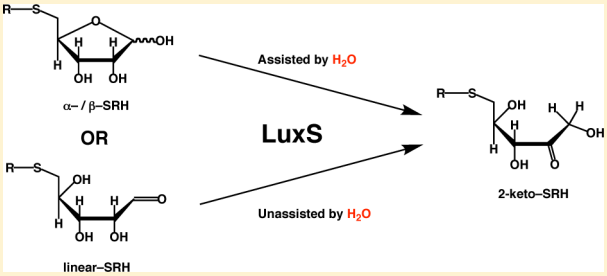

1. INTRODUCTION

Traditionally, antibiotics are used in the treatment of bacterial infections in order to kill or inhibit the growth of the pathogen. However, their extensive use has had a significant role in the emergence of antibiotic-resistant bacteria.[1] This is increasingly being recognized as a potential major public-health problem. Consequently, there is tremendous interest in identifying new therapeutic approaches to treating such pathogens. One promising approach is to render the pathogens harmless or reduce their efficacy, and allowing the host's immune system the time to adequately respond naturally to these pathogens.[2]

Type 2 quorum sensing (QS-2) is a cell-to-cell signaling process that regulates gene expression and ultimately population behavior via culture density.[3−5] The signaling molecule central to this process is the borate diester of cyclic 4,5-dihydroxy-2,3-petadione (DPD), otherwise known as autoinducer 2 (AI-2).[5,6] Detection of AI-2 by the microbes allows their populations to regulate diverse processes such as virulence, sporulation, motility, and biofilm formation.[2,7] The latter, in particular, has been shown to be involved in approximately 80% of all microbial infections, and plays a role in antibacterial resistance.[2,7,8] As QS-2 is not critical to the life-cycle of the bacteria, it is thought that it is not subject to the same degree of evolution-selective pressures.[7,9] Hence, inhibition of its biosynthesis has been suggested as a promising alternative approach for treating a broad range of pathogens.[2,10,11]

The biosynthesis of AI-2 is a multienzymatic process (Scheme 1).[5] It can be said to begin with demethylation of *S*-adenosylmethionine (SAM) by methyltransferase, thereby generating *S*-adenosylhomocysteine (SAH). *S*-Adenosylhomocysteine nucleosidase (Pfs) then removes the adenine moiety from SAH to produce *S*-ribosylhomocysteine (SRH) which is catalytically converted by *S*-ribosylhomocysteinase (LuxS) into homocysteine and 4,5-dihydroxy-2,3-pentadione (DPD). Importantly, the latter enzyme LuxS is found in a diverse array of pathogenic bacteria species but is not expressed in humans.[12] Hence, it represents a potential target for the inhibition of AI-2 biosynthesis and by extension QS-2.[13]

There have been a number of detailed experimental studies on the nature and mechanism of LuxS. In particular, it has been shown to be a dimeric nonheme iron metalloenzyme with its active sites located at the interface between its two monomers, both contributing residues to each active site.[9,10,13−15] Furthermore, the divalent Fe(II) ion is bound to the enzyme in a tetrahedral-like arrangement via two histidyl (His54, His58) and a cysteinyl (Cys126) residue.[15−17] In the absence of substrate, based on an X-ray crystal structure of a Zn(II)-containing inactive form of the enzyme (PDB ID: 1J6V),[10] the fourth ligand is thought to be an H_2O.[15] It should be noted that

Received: May 23, 2012
Revised: June 28, 2012
Published: June 28, 2012

dx.doi.org/10.1021/jp3049907 | *J. Phys. Chem. B* 2012, 116, 8916−8929

Scheme 1. Illustration of the Enzymatic Pathway of AI-2 Biosynthesis

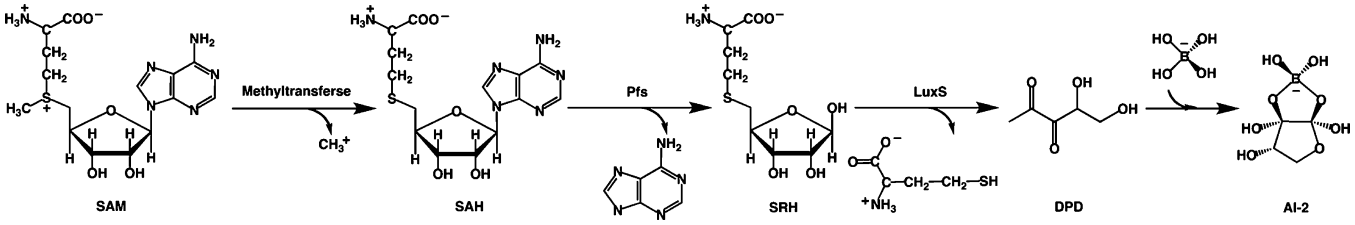

Scheme 2. The Proposed Catalytic Mechanism of LuxS[19]

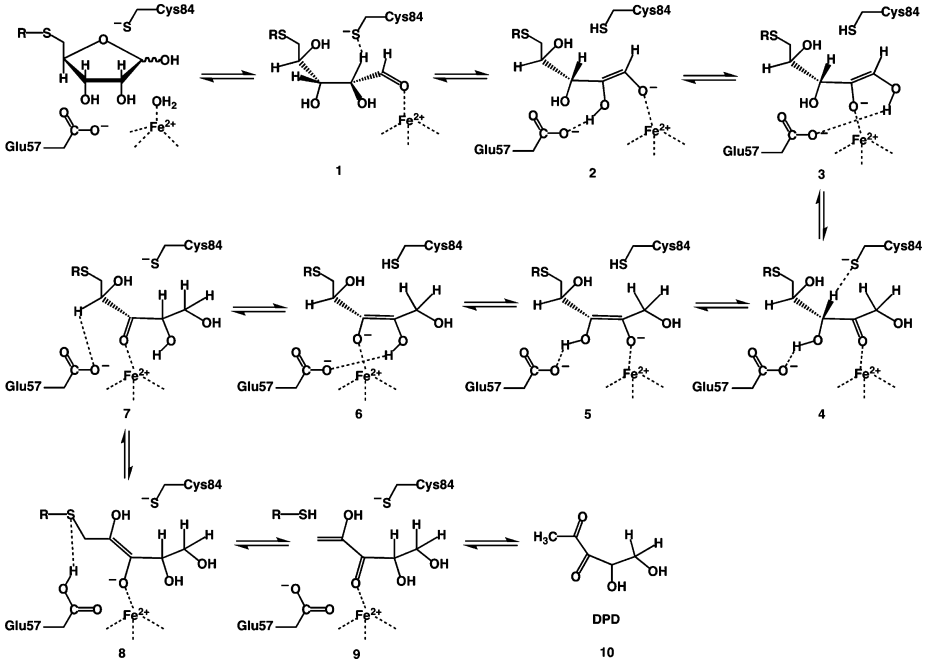

the numbering used herein is taken from that of *Bacillus subtilis* LuxS (PDB ID: 1YCL).[15] UV−vis spectroscopy has been used to examine ionization states of various active site residues. Importantly, they concluded that an active site cysteine (Cys84) is in its anionic form (i.e., Cys84−S^-), while a nearby arginyl residue (Arg39) is protonated and likely involved in stabilizing the thiolate.[9] In addition, X-ray crystallographic structures have been obtained of furanose-containing SRH bound within the active site of a LuxS in which Cys84 has been oxidized to sulfonic acid while the metal ion is Zn(II).[17] Furthermore, others have been obtained of the catalytically viable 2-keto derivative (2-keto-SRH), which contains a linear ribosyl moiety, bound within the active site of a Cys84Ala mutated LuxS containing a Co(II) ion. In the former, the substrate's cyclic ribosyl moiety was positioned "adjacent to" the Zn(II) ion,[17] while in the latter the noncyclic ribosyl was ligated to the Co(II) via its C2═O carbonyl oxygen.[15]

The kinetics of its mechanism have been investigated via ^{13}C NMR and UV−vis spectroscopy using the SRH substrate itself and the catalytically viable substrate derivatives 2- and 3-keto-SRH.[18,19] It was concluded that overall it proceeds in three distinct reaction stages.[19] Site-directed mutagenesis studies have examined the catalytic importance of several active site residues including Ser6, His11, Arg39, Cys84, and Glu57.[9,16,18−20] It was observed that, while the Cys84Asp mutation decreased the rate of reaction, a Cys84Ala substitution completely inhibited its activity.[18,19] In addition, Glu57 was shown to be important throughout the reaction but more so for catalytic turnover starting from the putative 3-keto-SRH intermediate, i.e., for the later stages of the mechanism.[19] Kinetic isotope studies into the stereo- and regio-chemistry of mechanistic proton transfers suggested that reaction of 2-keto-SRH to give the subsequent 3-keto-SRH intermediate was partially rate-limiting.[20] It has also been suggested that His11 may help transfer the C2−OH proton onto the C1−O oxygen with or without the help of other active-site residues and solvent molecules in the initial stage of the mechanism.[15,19]

On the basis of such observations, a catalytic mechanism for LuxS has been proposed and is shown in Scheme 2.[9,15−20] Importantly, while it was noted that in solution ribose preferably exists in its furanose form rather than as a linear aldose,[15,21] it was suggested that the ribosyl moiety in SRH must be linear in order for catalysis to occur.[9] In this linear aldose configuration, SRH is proposed to bind to the Fe(II) ion via its C1═O oxygen (**1**). The Cys84 thiolate then abstracts a proton from the substrate —C2H— group and transfers it onto the adjacent C1 carbon with concomitant transfer of the —O2H proton onto the O1 center (Scheme 2: **1** → **2** → **3** → **4**). The resulting 2-keto-SRH derivative (**4**) formed ligates via its C2═O oxygen to the Fe(II), as observed in the corresponding X-ray crystal structure (PDB ID: 1YCL).[15] This is then followed by the analogous reaction in which the Cys84 thiolate, having been regenerated upon protonation of the C1 center, facilitates a 1,2-proton transfer from —C3H—

dx.doi.org/10.1021/jp3049907 | J. Phys. Chem. B 2012, 116, 8916−8929

Scheme 3. Illustration of the Structures of the 2-keto-ribose Intermediate and Different Substrate and Substrate-Analogues (See Text)

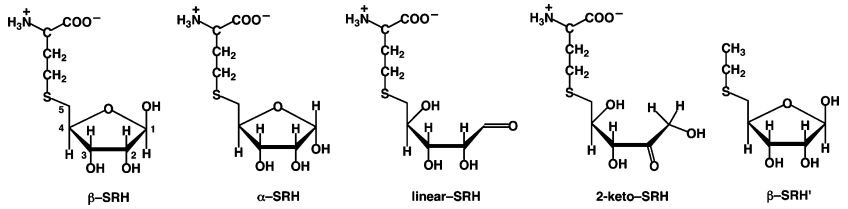

onto the adjacent —C2— carbon (i.e., **4** → **5** → **6** → **7**). Similarly, this occurs with transfer of the —O3H proton onto O2 to give the 3-keto-SRH derivative (Scheme 2). Subsequent cleavage of the substrate's thioester C—S bond (i.e., **7** → **8** → **9**) is achieved via a Glu57 assisted 1,3-proton transfer. Specifically, it abstracts a proton from —C4H— in **7** and transfers it onto the sulfur of the cleaving C—S bond, i.e., the homocysteine leaving group. This results in formation of homocysteine (Hcys) and DPD, the latter ultimately being converted into AI-2.

Unfortunately, many key fundamental questions still remain including the exact nature of the initial bound SRH substrate and how LuxS may facilitate conversion of the α- and/or β-furanose-containing SRH anomers into their corresponding linear aldose forms for further reaction as proposed.[19,22] Knowledge of substrate binding is highly pertinent for elucidating and understanding an enzyme mechanism and, for example, inhibitory studies. In particular, it can provide invaluable insights into key catalytic interactions between the substrate and the enzyme's active site functionalities (e.g., residues, waters, and cofactors) and, consequently, potential initial reaction steps. Hence, in this study, several complementary computational methods have been synergistically applied to investigate the initial stages of the proposed catalytic mechanism of LuxS. Specifically, docking and molecular dynamics (MD) simulations and an ONIOM QM/MM approach have been used to examine the nature of the initial active-site-bound substrate and the initial steps of the catalytic mechanism of LuxS leading to formation of the proposed 2-keto-SRH intermediate.

2. COMPUTATIONAL METHODS

Docking and Molecular Dynamics (MD) Simulations. These calculations were performed using the Molecular Operating Environment (MOE) software package.[23] The initial LuxS−substrate complex was obtained by appropriately modifying the X-ray crystal structure of catalytically inactive Cys84Ala Co(II)−LuxS (PDB ID: 1YCL) with the putative 2-keto-ribose (2-keto-SRH) intermediate bound within its active site.[15] Specifically, for one of the active sites, the Ala84 residue and Co(II) were replaced by a cysteinyl and Fe(II) ion, respectively, thus regenerating the wild type active site.[16] The bound 2-keto-SRH moiety in the crystal structure was used as a template to generate the structure of a "linear aldose SRH" (Scheme 3: linear-SRH). For binding of the α- and β-furanose-containing anomers of SRH (α-SRH and β-SRH), the 2-keto-SRH and all water molecules were removed from the crystal structure and the substrate analogue 5-*S*-ethyl-5-thio-D-β-ribofuranose (Scheme 3: β-SRH′) was then docked using a Proxy Triangle placement approach in conjunction with the London dG scoring function. The top 30 complexes were then refined using the AMBER99 force field and rescored with the London dG scoring function.[24,25] The top scoring complex was then selected for further analysis. Initial structures of the enzyme···α-/β-SRH complexes were generated by appropriately replacing β-SRH′ in the above optimized structure with α- and β-SRH, respectively.

The four chemical models of LuxS with α-SRH, β-SRH, linear-SRH, and 2-keto-SRH (Scheme 3) bound were solvated in a 7 Å spherical layer of water molecules. The damping functional factors included in the electrostatic and van der Waals potentials were set to decay smoothly beyond 8−10 Å. A spherical potential wall with a scaling constant of 2 was placed around each complex. The resulting solvated structures were then minimized using the AMBER99 force field[25] until the root-mean-square gradient of the total energy fell below 1 kcal mol^{-1} $Å^{-1}$. They were then annealed at the same level of theory under constrained pressure and temperature with the equations of motion coupled to a Nosé−Poincaré−Andersen thermostat[23] and a time step for numerical integration of 2 fs. The complexes were then heated and cooled using our previously published protocol of gradually raising the temperature from 150 to 400 K and then lowering to 300 K (Table S1, Supporting Information).[24] It should be noted that structures obtained from this process were also compared where possible to appropriate available X-ray crystal structures to help ensure they correctly reflected experimentally observed features.

The final four annealed structures obtained were then used as the starting points for subsequent 3.5 ns MD simulations. However, now only those residues within 13.5 Å of the substrate or intermediate ribosyl moiety were free to move. The simulations were performed using the AMBER99 force field[25] within the same parameters and convergence criteria as noted above but at a constant temperature of 300 K.

QM/MM Calculations. The Gaussian 09 program[26] was used for all two-layer ONIOM QM/MM calculations. Optimized structures and their corresponding harmonic vibrational frequencies were obtained at the B3LYP/6-31G-(d,p) level of theory for the QM layer and the AMBER96 force field for the MM layer, within the mechanical embedding (ME) formalism, ONIOM(B3LYP/6-31G(d,p)//AMBER96)-ME.[25,27−30] Relative energies were obtained via single point energy calculations at the ONIOM(B3LYP/6-311+G(2df,p)//AMBER96)-ME level of theory on the above optimized structures.[30−32]

The chemical model used was taken from the X-ray crystal structure of a mutated LuxS with the catalytically viable 2-keto-SRH putative intermediate bound (PDB ID: 1YCL).[15] The chemical model used, with 2-keto-SRH bound, is shown in Figure 1.[15] More specifically, the QM layer included the substrate's 5-*S*-ethyl-5-thio-D-ribofuranose moiety, the Fe(II) ion, and the R-groups of His54A, His58B, and Cys126A to which it is ligated. In addition, the R-groups of the active site residues Cys84B, Glu57A, and Ser6B were included as well as

dx.doi.org/10.1021/jp3049907 | J. Phys. Chem. B 2012, 116, 8916−8929

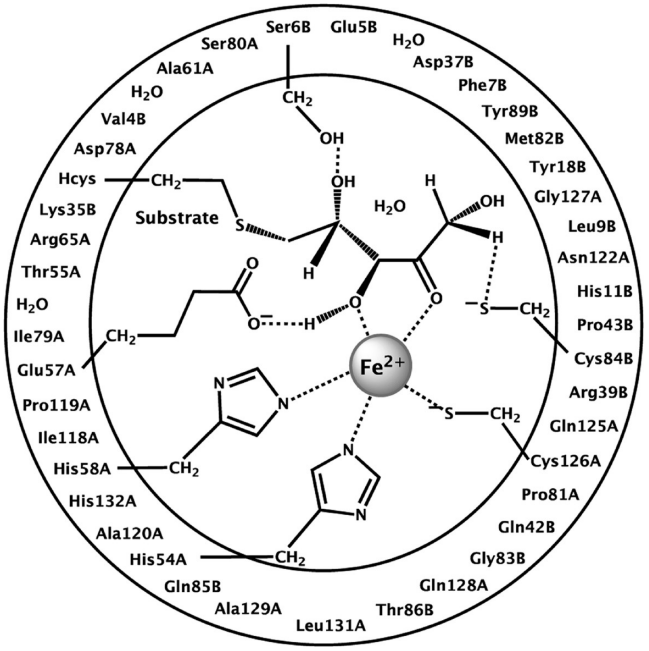

Figure 1. Schematic illustration of the ONIOM QM/MM active-site-containing chemical model with 2-keto-SRH bound: the inner circle indicates those moieties included in the QM region, while the outer circle indicates those residues and H_2O's included in the MM layer.

an active site water molecule. The residues for the MM layer were chosen, and included in their entirety, on the basis that together they fully surround the QM layer. Several H_2O molecules that interact electrostatically with QM layer constituents were also included. In order to ensure the integrity of the model, a minimal number of select atoms were held fixed at their X-ray crystal structure position (Table S2, Supporting Information).

3. RESULTS AND DISCUSSION

3.1. Docking and MD Simulations. Due in part to the fact that there is an experimental X-ray crystal structure (PDB ID: 1YCL) available for comparison, we began the docking and MD simulation studies on substrate binding by examining the enzyme···2-keto-SRH intermediate complex. It should be noted that rather than consider the entire complex we have focused on the dynamic behavior of the substrate/intermediate itself and several key active site residues and the active site water. Specifically, we considered the root-mean-square deviations (rmsd's) of the heavy atoms of those chemical functionalities in the QM region of the QM/MM model (see Figure 1) during the 1−3.5 ns time period of the simulations.

3.1.1. The Active-Site-Bound 2-keto-SRH Intermediate Complex. Within the bound active site complex, it is possible that the enzyme residues and the substrate are not equally fluxional in their behavior. That is, the residues may be quite rigidly oriented while the substrate is more mobile, or vice versa. This behavior can be seen in their respective rmsd's over the course of the simulation. Hence, in Figure 2, for the active-site-bound 2-keto-SRH complex, time is plotted versus the rmsd's of (i) the entire QM region (rmsd-QM), (ii) the residues and active site water in the QM region (rmsd-QM-residues), and (iii) the bound 2-keto-SRH intermediate (rmsd-substrate) itself. It is noted that the potential energy (U) of the system was very stable during the 3.5 ns simulation. It should be noted that the rmsd's shown are relative to the initial structure (see Computational Methods) of the bound complex at time t = 0.0 ps.

In the plot of rmsd-QM versus time (Figure 2a), it can be seen that the rmsd-QM's generally lie in the reasonably broad range of 0.15−0.5 Å and the bound active site *as a whole* shows a notable degree of fluxional behavior. That is, there is marked mobility in the positions of at least some atoms of the QM region during the course of the MD simulation. However, it does not tell us whether this observed mobility arises from the residues or possibly the 2-keto-SRH intermediate itself.

In Figure 2b, the rmsd's of only the nonsubstrate moieties in the QM region (rmsd-QM-residues), which includes the active site residues and water molecule, are plotted against time, while in Figure 2c the rmsd's of only the 2-keto-SRH moiety are plotted against time. In general, the rmsd-QM-residues lie in the relatively narrow range of 0.14−0.32 Å, indicating that they are relatively stably positioned during the simulation. In contrast, however, the 2-keto-SRH moiety shows significant fluctuations in its calculated rmsd's over the course of the simulation, ranging from ∼0.08 to 0.85 Å. This clearly indicates that the large fluctuations observed in Figure 2a, i.e., the rmsd's of the entire QM region, are due predominantly to the 2-keto-SRH intermediate itself.

In order to gain further insight into which atom(s) within the 2-keto-SRH moiety are most mobile, and by extension possible active site···intermediate interactions, we performed a cluster analysis of the rmsd-QM, i.e., of the entire "QM region". Specifically, the rmsd-QM results were grouped into five clusters and an average structure for each cluster obtained. These structures were then overlaid with each other and are shown in Figure 3. It should be noted that the average structures obtained were in good overall agreement with the experimentally determined X-ray crystal structure (PDB ID: 1YCL).

The overlaid structures shown in Figure 3 clearly show those atoms or groups that vary least and those that vary most in their positioning during the MD simulations, and thus provide insight into the above plots (see Figure 2). One can see that the active site residues do not vary greatly in their positioning. However, large variability is seen in several groups within the 2-keto-SRH moiety. More specifically, in approximately half of the structures, its −O1H group hydrogen bonds to the imidazole of His11, while in the other half it is instead intramolecularly hydrogen bonded with the 2-keto-SRH's own −O4H hydroxyl. It is noted that these two alternative binding modes of −O1H give rise to two average distances between O1 and the nearest imidazole nitrogen of His11 (His11−N) of 2.8 and 3.6 Å. These values bracket the corresponding distance observed in the experimental X-ray crystal structure of 3.04 Å. The 2-keto-SRH −O4H hydroxyl is itself quite consistently directed toward the sulfur of the homocysteine moiety. However, the variability of its positioning may reflect in part the mobility of the sulfur (see Figure 3).

Perhaps more importantly, it can be seen that the 2-keto-SRH's O2 and O3 centers are consistently ligated to the Fe(II) ion over the period of the simulation with average distances of 2.24 and 2.30 Å, respectively. Meanwhile, the −O3H hydroxyl maintains a hydrogen bond with the carboxylate of Glu57. It is noted that the average Glu57−COO^-···O3 distance of 2.67 Å is in good agreement with that observed in the X-ray crystal structure (PDB ID: 1YCL) of 2.51 Å. Furthermore, the average distance between the thiolate of Cys84 and the substrate's C3,

dx.doi.org/10.1021/jp3049907 | J. Phys. Chem. B 2012, 116, 8916−8929

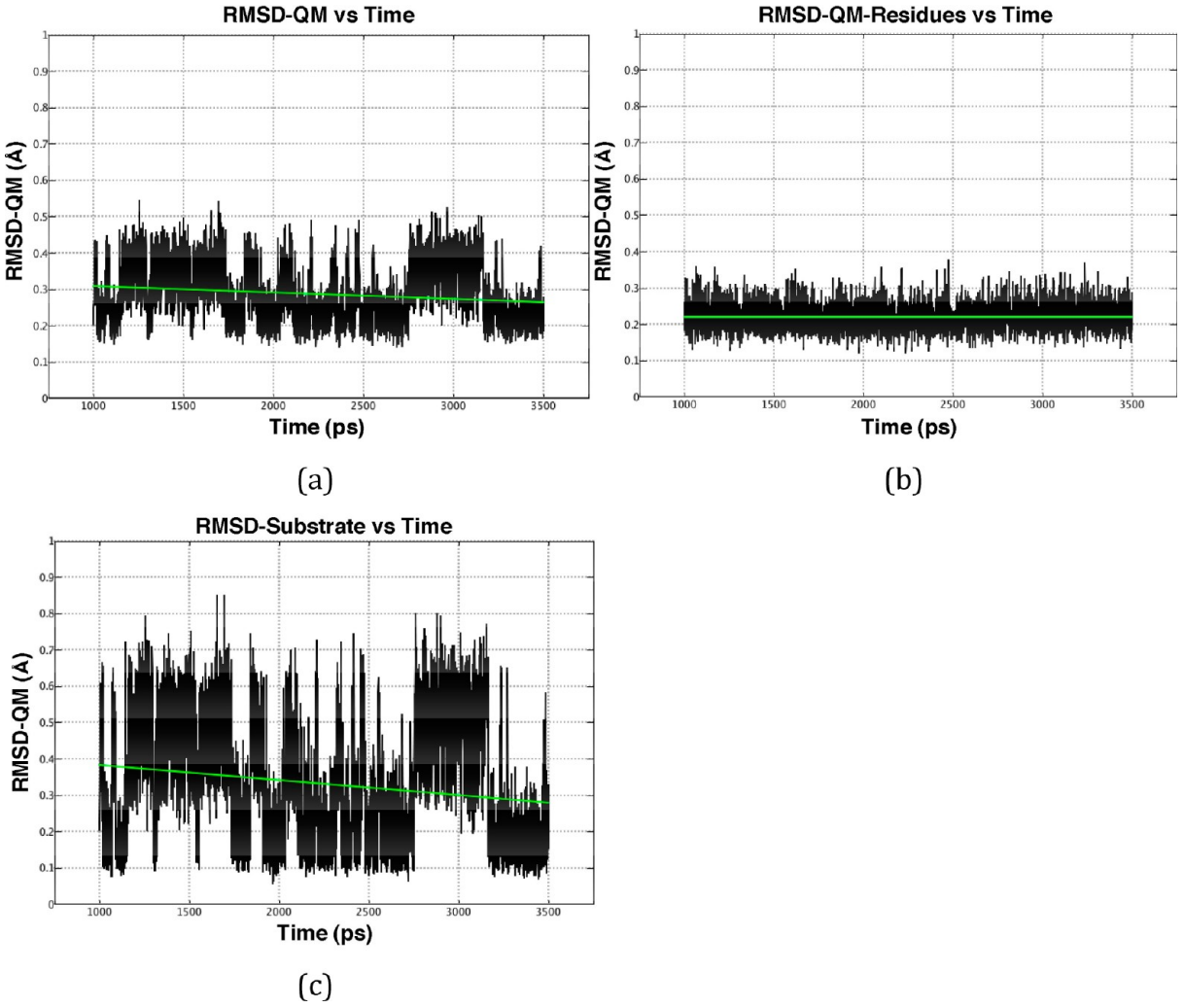

Figure 2. Plots of rmsd's calculated during the MD simulations for the enzyme···2-keto-SRH intermediate complex: (a) rmsd-QM versus time (ps); (b) rmsd-active site residues versus time (ps); (c) rmsd-substrate versus time (ps).

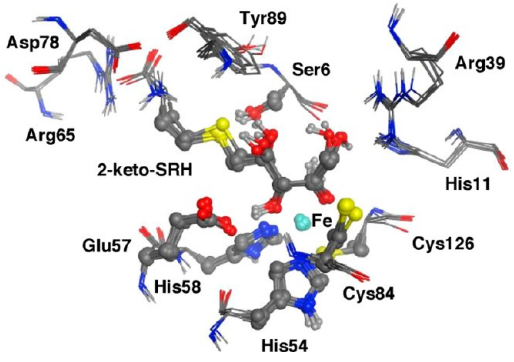

Figure 3. Overlay of select residues and active site moieties of the five average structures obtained from cluster analysis of rmsd-QM's of the active-site-bound 2-keto-SRH complex. For clarity, only selected hydrogen atoms are shown. Color key: C (gray); O (red); N (blue); S (yellow); H (white); Fe (aqua).

C2, and C1 atoms is 4.47, 3.75, and 3.48 Å, respectively. Given r(CH3S−H) = 1.33 Å,[33] it appears that both supposedly mechanistically important acid/base groups are positioned for their respective proposed proton abstraction roles. A positional change or reaction of the 2-keto-SRH may be required to facilitate proton transfer from −C3H− to the Cys84 thiolate in the next stage of the mechanism.

3.1.2. The Active-Site-Bound β- and α-SRH Complexes. We then proceeded to examine the active-site-bound substrate complexes in which the ribosyl sugar within the SRH substrate was in either its α- or β-furanose configuration, α- and β-SRH, respectively.

For the β-SRH···enzyme complex, the plot of rmsd's for the active-site-bound substrate region versus time is given in Figure 4a. In contrast to that observed for the above active-site-bound 2-keto-SRH intermediate complex (cf. Figure 2), over the period of the simulation, the majority of the points now lie within a much narrower range: approximately 0.17−0.38 Å. This suggests that the configuration of the "QM-region" of the enzyme is quite consistent with only relatively modest changes observed in the positions of atoms and/or groups.

The five average structures obtained by performing a cluster analysis on the rmsd-QM's are shown overlaid in Figure 4b. In agreement with that indicated by Figure 4a, it can be seen that there is much less variation in the positions and orientations of various active site and substrate functional groups. Notably, both the O2 and O3 ribosyl oxygens of β-SRH are consistently ligated to the Fe(II) center with average Fe(II)···O distances of 2.30 and 2.26 Å, respectively. These lengths are similar to that

dx.doi.org/10.1021/jp3049907 | J. Phys. Chem. B 2012, 116, 8916−8929

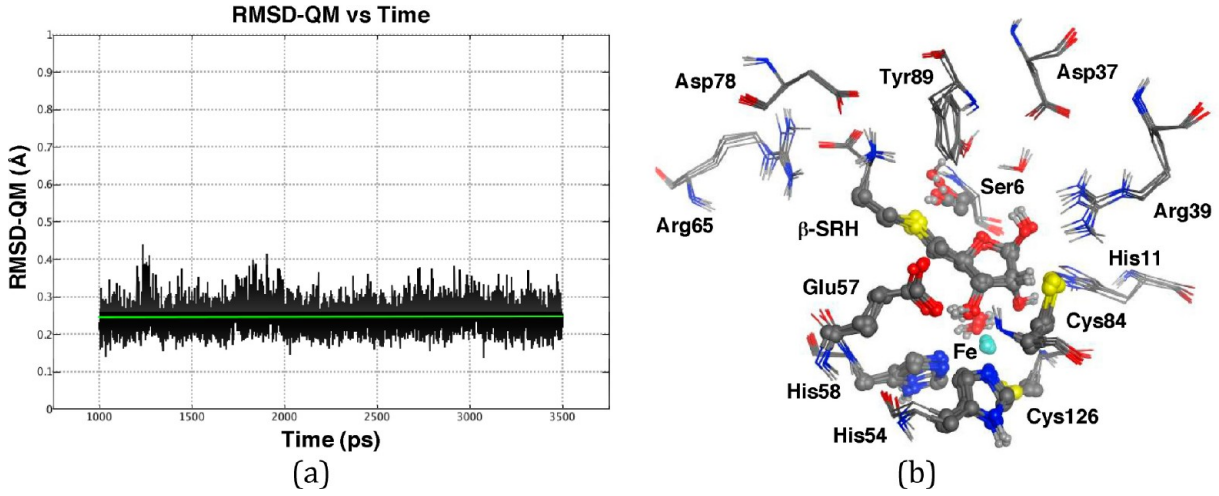

Figure 4. For the active-site-bound β-SRH substrate complex: (a) plot of rmsd-QM versus time (ps) and (b) overlay of the five average structures obtained from cluster analysis of the rmsd-QM. Color key: C (gray); O (red); N (blue); S (yellow); H (white); Fe (aqua).

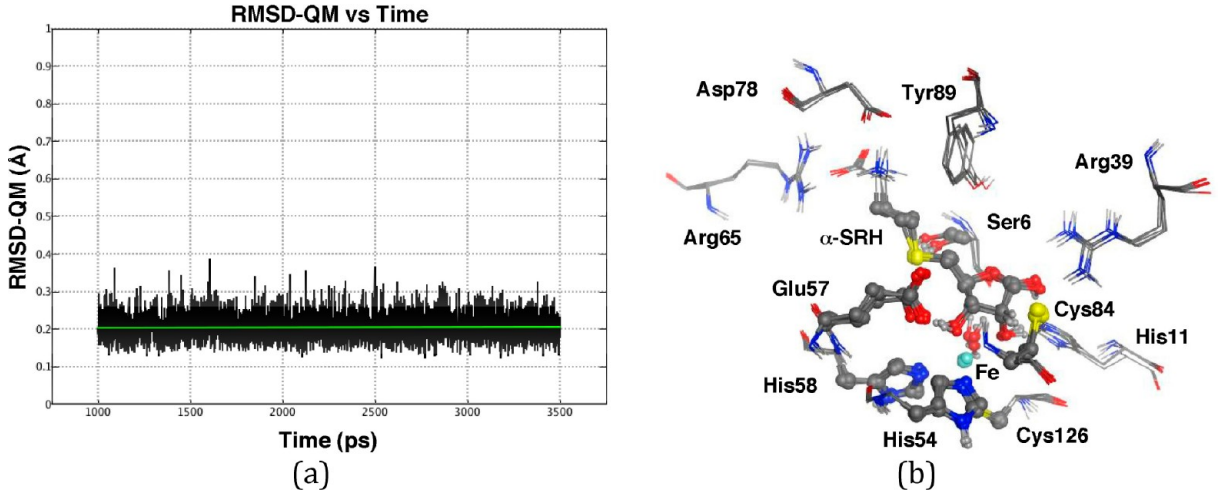

Figure 5. For the active-site-bound α-SRH substrate complex: (a) plot of rmsd-QM versus time (ps) and (b) overlay of the five average structures obtained from cluster analysis of the rmsd-QM. Color key: C (gray); O (red); N (blue); S (yellow); H (white); Fe (aqua).

obtained above for the corresponding interactions in the 2-keto-SRH intermediate complex. In addition, the −O1H hydroxyl is hydrogen bonded to the R-group carboxylate of an aspartyl residue (Asp37) via a bridging water molecule, while the R-group hydroxyl of Ser6 hydrogen bonds to the substrate's sulfur (Figure 4b). Importantly, the carboxylate of Glu57 again maintains a consistent strong hydrogen bonding interaction with the substrate's −O3H group. This is illustrated by the fact that in all five structures the −O3H proton is directed toward an oxygen of the carboxylate of Glu57 with an average Glu57−COO^-···O3 distance of just 2.52 Å. Furthermore, Cys84 is located near the ribose's −C2H− group with an average Cys84−S^-···C2 distance of 2.70 Å. Hence, both proposed mechanistic acid/base groups, Glu57 and Cys84, appear suitably positioned for proton abstraction from the −O3H and −C2H− groups, respectively.

For the alternate enzyme···α-SRH complex, the plot of rmsd's for the active-site-bound substrate region versus time is given in Figure 5a. Similar to that observed for the enzyme···β-SRH complex, the plot of RSMD-QM versus time clearly indicates that the active site and bound substrate are again quite consistent in their positioning throughout the simulation with the majority of points lying within the quite narrow range of 0.15−0.3 Å.

The five average structures obtained from a cluster analysis of the rmsd-QM analysis are shown overlaid in Figure 5b. As can be seen, the active site residues are quite static in their positioning while the substrate's ribosyl moiety is consistently ligated to the Fe(II) center via both its O2 and O3 oxygens with average distances of 2.27 and 2.25 Å, respectively. As observed for the active site bound alternate anomer β-SRH, these distances are in reasonable agreement with those calculated for the active-site-bound 2-keto-SRH intermediate complex. Similarly, the −O3H hydroxyl in all structures is strongly hydrogen bonded to the Glu57 R-group carboxylate, as indicated by its very short average Glu57−COO^-···O3 distance of 2.49 Å. In addition, the thiolate sulfur of the other proposed active site base/acid Cys84 is situated near the ribose moiety's −C2H− proton with an average Cys84−S^-···HC2 distance of 2.50 Å.

As might be expected, the main differences seen between binding of the α- and β-anomers of the SRH substrate involves the groups on C1, in particular, the −O1H hydroxyl group. In contrast to that observed for the bound β-SRH substrate, on

dx.doi.org/10.1021/jp3049907 | J. Phys. Chem. B 2012, 116, 8916−8929

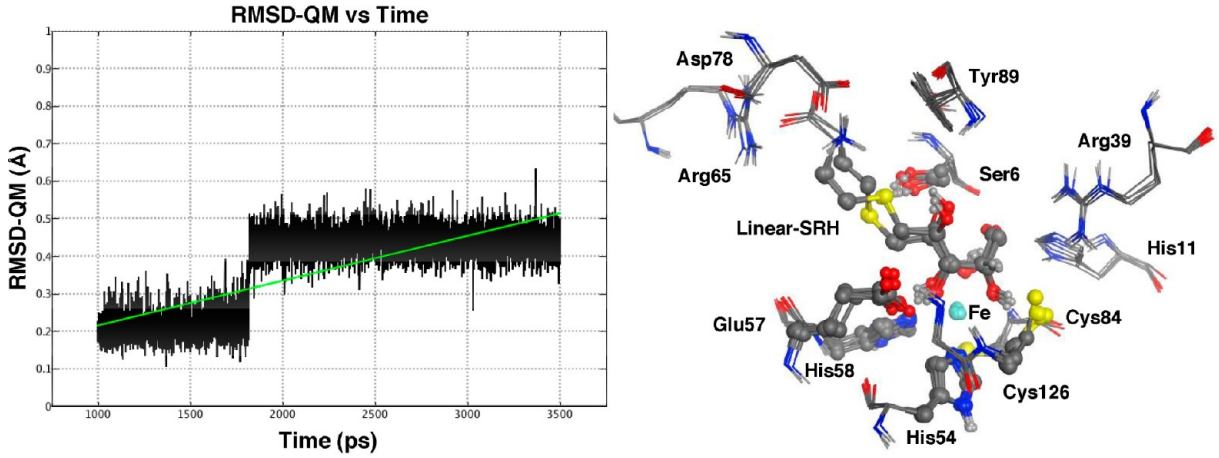

Figure 6. For the active-site-bound linear aldose SRH substrate (linear-SRH) complex: (a) plot of rmsd-QM versus time (ps) and (b) overlay of the five average structures obtained from cluster analysis of the rmsd-QM. Color key: C (gray); O (red); N (blue); S (yellow); H (white); Fe (aqua).

binding of α-SRH, the −O1H group hydrogen bonds to the basic nitrogen of the R-group imidazole of His11 with an average distance of 2.20 Å. In addition, the protonated R-group guanidinium of Arg39 also strongly interacts with the −O1H oxygen; average $r(\text{Arg39}-\text{NH}_2^+\cdots\text{O1})$ = 2.76 Å.

3.1.3. The Active-Site-Bound Linear Aldose−SRH Complex. It is proposed[19] that the SRH ribosyl moiety must be in its linear aldose configuration (i.e., contain a −C1HO group; see Scheme 3) in order for the catalytic mechanism to proceed (see Scheme 2). Potentially, this may be formed via ring-opening of the above furanose-containing α- and β-SRH upon their interaction with LuxS or may be formed within the aqueous solution and then binds within the LuxS active site.[22] Thus, we also examined the binding of such a "linear-SRH" moiety. The rmsd-QM's obtained from the MD simulation of the active-site-bound linear-SRH complex are plotted against time in Figure 6a. It can be seen that the resulting complex is much more dynamic with two distinct regions observed in the measured rmsd's. The first exists in the period of 1−1.8 ns with a range of rmsd's of 0.15−0.35 Å, while the second begins at 1.8 ns and lasts for the remainder of the simulation. For this latter region, the rmsd-QM's now mostly lie in the approximate range of 0.35−0.55 Å (Figure 6a). It is noted that the MD simulation was continued for a further 10 ns in order to further consider interconversion between these two conformations (Figure S1, Supporting Information). Importantly, no other conformation was observed; the above two interconverting between each other with that corresponding to the rmsd range 0.35−0.55 Å being predominate.

As for the previous complexes, we then performed a cluster analysis, as described above, of the rmsd-QM's shown in Figure 6a. For each of the five clusters, an average structure was obtained and then overlaid with each other, as shown in Figure 6b. As for the above possible bound substrate and 2-keto-SRH intermediate complexes, the active site residues are quite localized with little positional movement observed over the course of the simulation. Similarly, the ribosyl moiety O2 and O3 oxygens are ligated to the Fe(II) ion with average distances of 2.36 and 2.28 Å, respectively, while the R-group carboxylate of Glu57 forms a short strong hydrogen bond with the ribose's —O3H group; average $r(\text{Glu57}—\text{COO}^-\cdots\text{O3}—)$ = 2.52 Å. In contrast to that observed in both the bound α- and β-SRH complexes (see above), the Cys84 thiolate no longer sits above the ribose moiety and the —C2H— group. In contrast, it forms a strong hydrogen bond with the ribose's —O2H hydroxyl with an average $r(\text{Cys84}—\text{S}^-\cdots\text{HO2}—)$ = 2.05 Å. This altered mechanistic base−substrate interaction could affect the ability of Cys84—S^- to act as a base to deprotonate the —C2H— group, the initial reaction in the proposed mechanism. It is likely due in part to this altered Cys84···substrate interaction that, unlike in the above enzyme−substrate complexes containing a furanose moiety, neither Arg39 nor His11 interact with the substrate. The C1═O carbonyl oxygen instead hydrogen bonds with the water ligated to the Fe(II) ion.

The jump in rmsd-QM's observed at ∼1.8 ns in Figure 6a, however, is principally due to the distinct conformational change that occurs in the −CH2CH2S− component of the homocysteine moiety of the substrate (Figure 6b). This change is not observed in the active-site-bound β- and α-SRH complexes (see Figures 4b and 5b) nor the bound 2-keto-SRH intermediate (see Figure 3c). This may be due in part to the linearity of the substrate and its fewer substrate−enzyme interactions and hence its greater flexibility than in the above three complexes.

3.2. QM/MM Investigation on the Catalytic Mechanism. *3.2.1. Active-Site-Bound Substrate Complexes.* The above MD simulations suggest that the SRH substrate may bind within the active site when its ribosyl moiety occurs as either an α- or β-furanose or as a linear aldose. Using a QM/MM approach, we then examined the structures and energies of four possible substrate-bound active site complexes: SRH in its α- or β-furanose (α-RC and β-RC) forms, and the corresponding linear aldose configurations (α-RC′ and β-RC′) which can be thought of as resulting from ring-opening of their respective furanose anomers. The optimized structures obtained with selected bond lengths given in angstroms are shown in Figure 7.

The optimized structures of the α-RC and β-RC complexes share a number of similarities but also exhibit several notable differences. For instance in both, as in their average MD structures, the sugar moiety of the SRH coordinates to the Fe(II) via its O2 and O3 centers (Figure 7). In α-RC, the Fe(II)···O2/O3 distances are 2.19/2.12 Å, while, in β-RC, the

dx.doi.org/10.1021/jp3049907 | J. Phys. Chem. B 2012, 116, 8916−8929

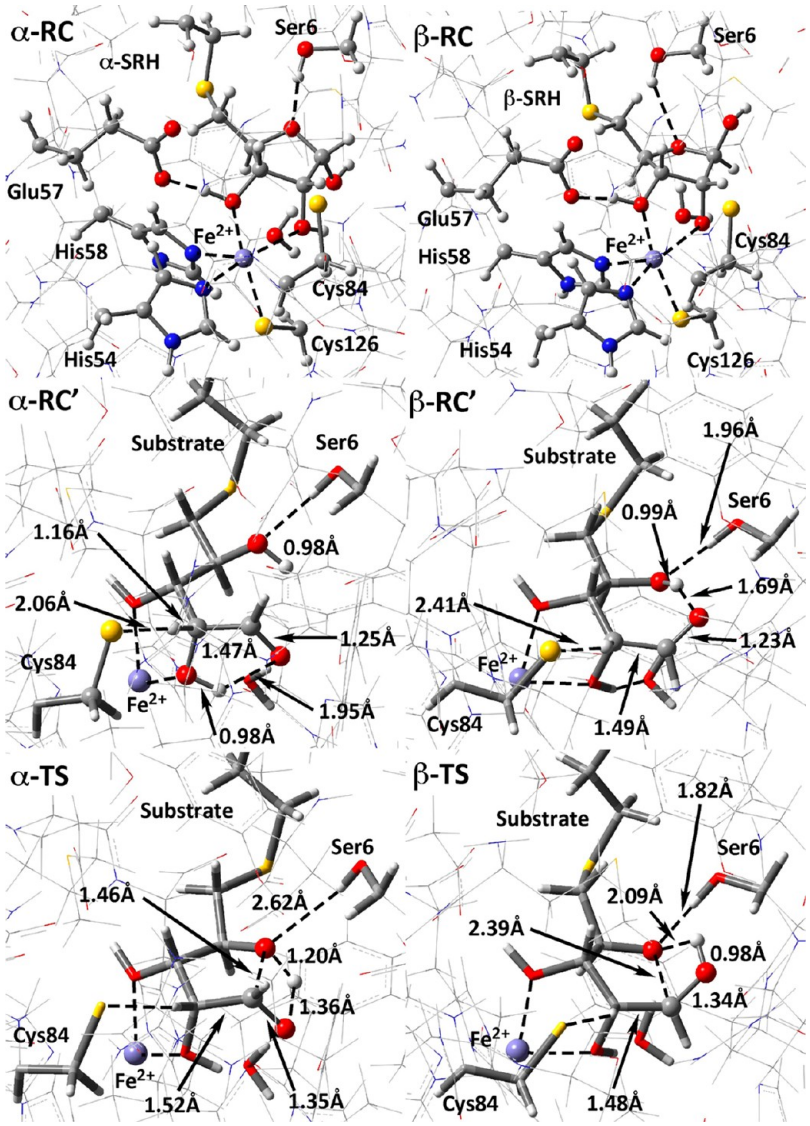

Figure 7. Optimized structures with selected bond distances (angstroms) of the active-site-bound SRH substrate complexes in which the substrate's ribose sugar is in its α- (α-RC) or β-furanose (β-RC) anomer or corresponding linear aldose configurations (α-RC′ and β-RC′), and transition structures for ring-opening α-TS and β-TS (see text). Color key: C (gray); O (red); N (blue); S (yellow); H (white); Fe (purple).

sugar is slightly more tightly ligated with interaction distances of 2.16/2.12 Å, respectively. In addition, in both complexes, the Ser6 R-group hydroxyl hydrogen bonds to the SRH's sugar ring oxygen (O4). However, in β-RC, it is markedly weaker with a Ser6−OH···O4 distance of 2.84 Å compared to just 2.03 Å in α-RC. In fact, in the former, the Ser6−OH is positioned closer to the substrate's sulfur.

Notably, in both complexes, the acid/bases, Cys84 and Glu57, appear well positioned for their proposed mechanistic roles. For instance, the thiolate of Cys84 interacts with the ribose's C2−H proton with Cys84−S^-···HC2 distances of 2.35 and 2.55 Å in α-RC and β-RC, respectively. Meanwhile, the carboxylate of Glu57 forms very short and strong hydrogen bonds with the ribose's C3−OH hydroxyl proton with Glu57−COO^-···HOC3 distances of 1.46 Å (α-RC) and 1.48 Å (β-RC). A water molecule is also found in the active sites of both α- and β-RC. In α-RC, it is hydrogen bonded to the sugar's O1 center with $r(OH_2\cdots O1)$ = 1.83 Å, while in β-RC it is hydrogen bonded to both the sugar's O2 and O4 centers with distances of $r(OH_2\cdots O2)$ = 1.72 Å and $r(OH_2\cdots O4)$ = 1.80 Å, respectively.

It is noted that these differences in substrate−enzyme interactions lead to modest differences within the ribose ring. Namely, in α-RC, the O4−C1 and C1−O1 bonds have lengths of 1.41 and 1.43 Å, respectively. In contrast, in β-RC, these bond lengths are now 1.46 and 1.39 Å, respectively. Thus, the former appears to have a more strongly bound ring, while, in the latter, the C1−O bond has partial double bond character and consequently the O4−C1 bond is lengthened.

Significantly, due to these binding and structural differences, the α-RC active-site-bound substrate complex is thermodynamically preferred, lying 47.5 kJ mol^{-1} lower in energy than β-RC.

The two possible initial "linear-SRH substrate" complexes were then considered. In α-RC′, the C1═O oxygen is directed down analogous to the C1—OH group in α-RC, while, in β-RC′, it is directed upward analogous to β-RC. It is noted that the former complex is analogous to that observed in the MD simulations. Both complexes exhibit similar enzyme···substrate interactions as observed in their corresponding complexes α-RC and β-RC, respectively. For instance, in α- and β-RC′, the

dx.doi.org/10.1021/jp3049907 | J. Phys. Chem. B 2012, 116, 8916−8929

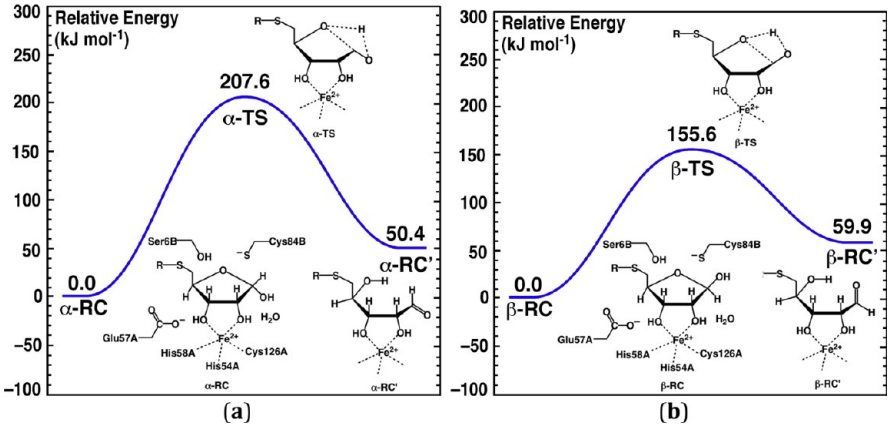

Figure 8. Schematic PESs for unassisted interconversion of (a) α-RC and α-RC′ and (b) β-RC and β-RC′.

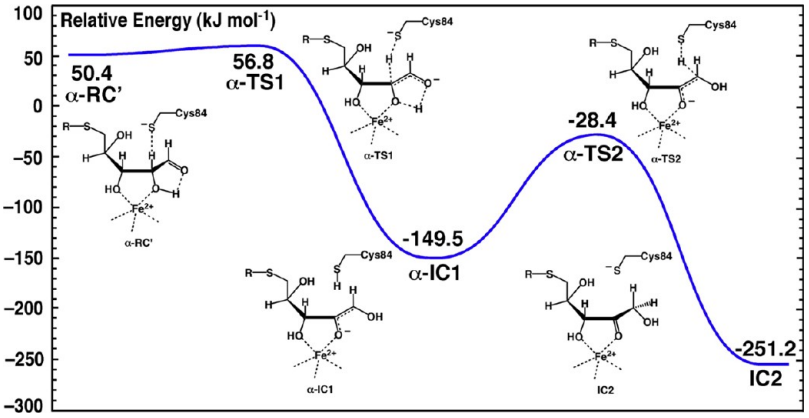

Figure 9. Calculated PES for reaction of the aldehyde-containing active-site-bound substrate complex α-RC′ to give the 2-keto-containing derivative IC2 (see text).

SRH moiety is again ligated via its O2 and O3 oxygens to the Fe(II) ion, while its O4 center is hydrogen bonded to the R-group hydroxyl of Ser6 (Figure 7). The latter, however, are now markedly shorter with Ser6-OH···O4 distances of 2.02 Å (α-RC′) and 1.96 Å (β-RC′). In α-RC′, the —O2H group is intramolecularly hydrogen bonded to the C1═O carbonyl oxygen. In contrast, in β-RC′, it is hydrogen bonded via the active site H_2O to O4 (Figure 7).

In α- and β-RC′, the Cys84 thiolate again interacts with the −C2H− proton, though now with markedly shorter distances of 2.06 and 2.41 Å, respectively. Similarly, the R-group carboxylate of Glu57 again strongly hydrogen bonds with its C3−OH protons with Glu57−COO^-···HOC3 distances of 1.51 Å (α-RC′) and 1.56 Å (β-RC′). Importantly, however, α-RC′ and β-RC′ lie decidedly higher in energy than α-RC by 50.4 and 107.4 kJ mol^{-1}, respectively! Furthermore, it should be noted that α-RC′ and β-RC′ are potentially able to interconvert via rotation about their C1−C2 bond.

3.2.2. Interconversion of Active-Site-Bound Substrate Complexes. The above results suggest that LuxS preferentially binds SRH containing an α- or β-furanose ring rather than the linear aldose (i.e., contain a C1═O group) form. However, as previously noted, it has been proposed that the SRH substrate must exist as the latter in order to undergo the subsequent reactions (Scheme 2). This suggests that α-RC and β-RC are able to interconvert with their analogous linear complexes α-RC′ and β-RC′, respectively; that is, α- and β-RC are able to undergo a ring-opening process.

There exists two possible approaches for formal transfer of the C1—OH proton onto the ring oxygen O4: (i) direct or unassisted transfer, or (ii) assisted transfer involving a nonsubstrate active site component. The potential energy surfaces (PESs) obtained for the former are shown in Figure 8. In the unassisted ring-opening process, the C1—OH proton directly transfers onto the ring oxygen O4. This results in ring-opening with formation of a —C1H═O aldehyde and an —O4H hydroxyl group. Such a reaction step necessarily requires a four-membered ring transition structure (TS), which are known to often be quite high in energy. Indeed, the ring-opening of α-RC to give α-RC′ proceeds via α-TS at a cost of 207.6 kJ mol^{-1} (Figure 8). Similarly, for the analogous conversion of β-RC to β-RC′ via β-TS, the barrier is quite high at 155.6 kJ mol^{-1}. Although this is lower than for α-RC/α-RC′, reflecting the structural differences noted in the initial anomeric furanose ring moieties above, it is still significantly higher than that considered the upper thermodynamic limit for an enzyme catalyzed reaction, ∼125 kJ mol^{-1}.[34] Thus, it appears that neither "unassisted ring-opening" process is likely to occur in LuxS.

Possible alternate pathways in which either an active site residue or water assists the ring-opening process were also examined. In both cases, however, there appears to be no suitable residue positioned to facilitate the proton transfer. Alternatively, the active site water near the ribosyl moiety observed in α- and β-RC (Figure 7) may be able to assist transfer of the C1−OH proton onto O4. Unfortunately, no

dx.doi.org/10.1021/jp3049907 | J. Phys. Chem. B 2012, 116, 8916−8929

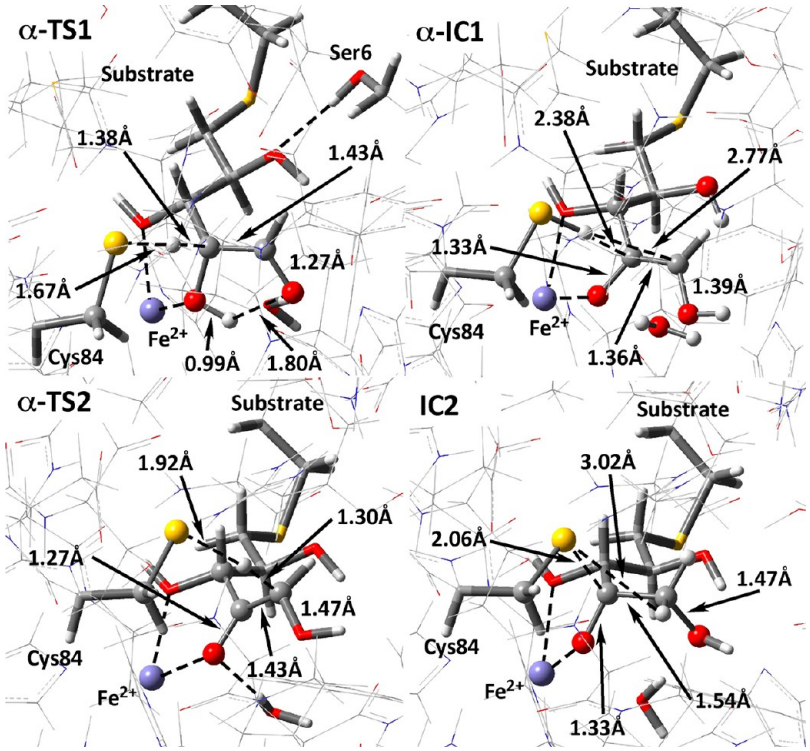

Figure 10. Optimized structures with selected bond distances (angstroms) of α-TS1, α-IC1, α-TS2, and IC2; see text. Color key: C (gray); O (red); N (blue); S (yellow); H (white); Fe (purple).

such pathway could be located for either system, all efforts leading to either the above four-membered ring TS or to TS's for an alternate ring-opening process (see below).

3.2.3. The Proposed Mechanism for Formation of the 2-keto-SRH Intermediate. In the proposed mechanism, the formation of the 2-keto-SRH intermediate from the bound linear aldose isomer occurs via involvement of Glu57. More specifically, it abstracts a proton from the ribosyl —O2H and transfers it onto the C1═O oxygen (O1). It has been alternatively suggested that this process may involve the —O2H transferring its proton via several residues onto His11, which then protonates O1.[15,19] In addition, Cys84—S^- assists transfer of a proton from the ribosyl —C2H— group onto the adjacent C1 (see Scheme 2). However, in the above structures of α- and β-RC′, the —O2H proton is directed away from Glu57. For completeness, and as the linear aldose SRH conformers may be bound by LuxS, possible pathways for their reaction to give a bound 2-keto-SRH intermediate were examined. The PES surface obtained for α-RC′ is shown in Figure 9, while optimized structures of stationary points along the pathway with selected bond lengths in angstroms are presented in Figure 10.

Due to the fact that in α-RC′ the ribose's −O2H group is hydrogen bonded directly to the O1 oxygen, proton transfer can occur via the five-member ring TS α-TS1 at a cost of just 6.4 kJ mol^{-1} with respect to α-RC′1 (Figure 9). This occurs with concomitant abstraction of the −C2H− by Cys84−S^-. This leads to formation of the −$O2^-$ oxyanion intermediate α-IC1 lying significantly lower in energy than α-RC′ by 199.9 kJ mol^{-1}, −149.5 relative to α-RC (Figure 7). In α-IC1, due to the increased oxyanion character of O2, the Fe(II)···O2 interaction has shortened significantly to 1.94 Å. However, while the C1−C2 bond has shortened (1.36 Å) as expected, a decrease in the C2−O2 length to 1.33 Å is also observed (Figure 10). This suggests that there is a degree of electron delocalization occurring among these bonds.

Formation of the corresponding 2-keto-SRH derivative from α-IC1 then occurs in one step by transfer of the Cys84-SH thiol proton onto the ribose's C1 center via α-TS2 with a markedly high relative cost to α-IC1 of 121.1 kJ mol^{-1} (−28.4 kJ mol^{-1} relative to α-RC). That is, the barrier for this single reaction step is near the upper thermodynamic limit for an enzymatic reaction.[34,35] The resulting bound 2-keto-SRH complex IC2 lies considerably lower in energy than α-RC′ by 301.6 or −251.2 kJ mol^{-1} relative to α-RC! It is noted that in IC2 the anionic Cys84−S^- sulfur sits quite close to the now quite electrophilic C2 center with r(Cys84−S^-···C2) = 2.06 Å. It should also be noted that a strong hydrogen bond is formed between −O1H and the basic nitrogen of the R-group imidazole of His11 (His11-N) with an average r(His11−N···HO1−) = 1.68 Å and r(His11−N···O1) = 2.64 Å. This His11−N···O1 distance is in good agreement with that observed in the crystal structure (3.04 Å; PDB ID: 1YCL) and the average distance (2.80 Å) observed in the MD simulation of the enzyme···2-keto-SRH complex.

Conversion of β-RC′ to its corresponding 2-keto-SRH derivative *is not* feasible via a pathway analogous to that above for α-RC′. This is because in β-RC′ the aldehyde oxygen O1 is *trans* to the ribose's −O2H group and, thus, direct proton transfer from −O2H onto O1 cannot occur. However, β-RC′ can first undergo a conformational rearrangement via rotation about its C1—C2 bond to give α-RC′ and then react as detailed above.

3.2.4. Alternative Mechanisms for Formation of the 2-keto-SRH Intermediate. The above results suggest that LuxS preferably binds the SRH substrate in which the ribose is in its furanose form, with the α-anomer being preferred. However, for both α- and β-RC, the reaction barriers for formation of the

dx.doi.org/10.1021/jp3049907 | J. Phys. Chem. B 2012, 116, 8916−8929

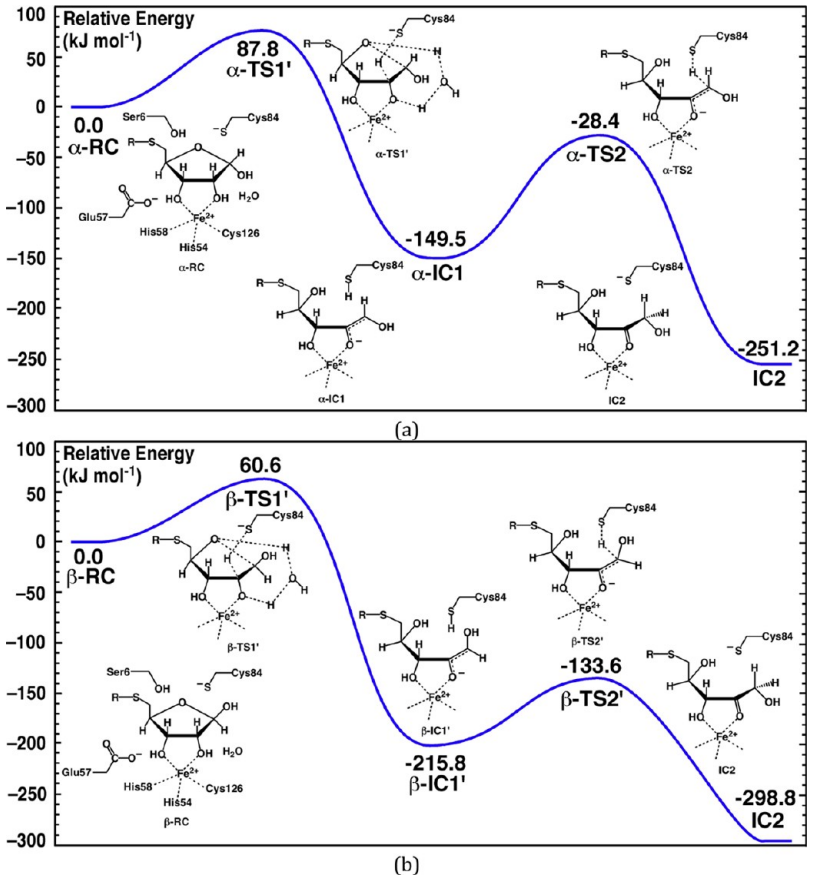

Figure 11. Calculated PESs for the alternate "water-assisted" pathway for reaction of (a) α-RC to give the 2-keto derivative IC2 and (b) β-RC to give the 2-keto derivative IC2.

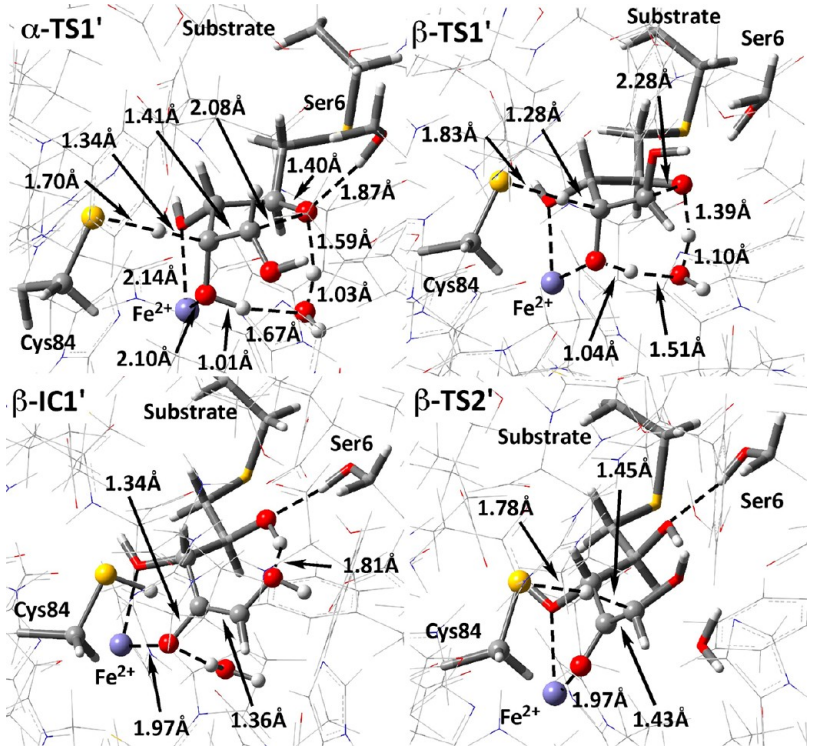

Figure 12. Optimized structures with selected bond distances (angstroms) of α-TS1′, β-TS1′, β-IC1′, and β-TS2′ (see text). Color key: C (gray); O (red); N (blue); S (yellow); H (white); Fe (purple).

dx.doi.org/10.1021/jp3049907 | J. Phys. Chem. B 2012, 116, 8916−8929

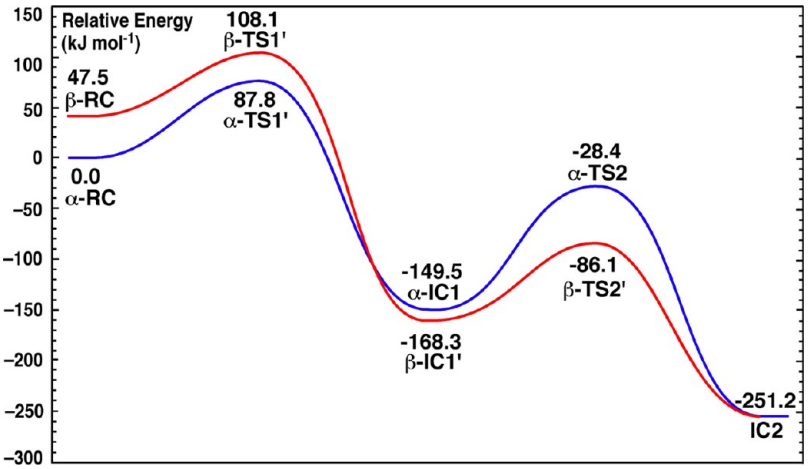

Figure 13. Comparison of the PESs for reaction of α-RC and β-RC via "water-assisted" ring-opening process alternative mechanisms.

bound linear-SRH complex (i.e., ring-opening) were enzymatically unfeasible (see Figure 8). Hence, possible alternative mechanisms for reaction of α- and β-RC to form a 2-keto-SRH intermediate were then examined.

In particular, it is noted that in the optimized structures of α- and β-RC the substrate's −O2H oxygen is ligated to the Fe(II) ion and, as a result, will be more acidic. Furthermore, in both complexes, the active site water is positioned "under" the ribose ring and could potentially act to facilitate proton transfer from −O2H onto the furanose ring oxygen O4. Such a process could potentially be independent of the anomeric character of the C1 carbon, i.e., α or β. The PESs obtained for the resulting "water-assisted" pathways for α- and β-RC are shown in Figure 11, while optimized structures with selected bond lengths in angstroms are given in Figure 12.

For α-RC, the transfer of the −O2H proton via the water onto O4 occurs with concomitant abstraction of the −C2H− proton by the Cys84 thiolate. This reaction step proceeds via α-TS1′ with a barrier of 87.8 kJ mol^{-1} and directly gives the energetically low-lying ring-opened 2-enolate intermediate α-IC1 described above. Importantly, it has been formed without the need to pass through the linear aldose complex α-RC′. The subsequent formation of the 2-keto-SRH complex IC2 then proceeds via α-TS2, as detailed above.

Similarly, for β-RC, transfer of the −O2H proton via the active site water onto O4 occurs with concomitant abstraction of the −C2H− proton by Cys84−S$^-$ to give the analogous ring-opened 2-enolate intermediate β-IC1′. This step proceeds via β-TS1′ at a cost of just 60.6 kJ mol^{-1} relative to β-RC, while β-IC1′ lies considerably lower in energy than β-RC by 215.8 kJ mol^{-1}. Structurally, β-IC1′ is similar to that of α-IC1 in that both the ribose O3 oxygen and the O2, which is formally an oxyanion, are ligated to the Fe(II) center with distances of 2.23 and 1.97 Å, respectively (Figure 12). Furthermore, again, electron delocalization is observed across the C2−C1 and C2−O2 bonds, as indicated by their bond lengths of 1.36 and 1.34 Å, respectively. In addition, an NBO population analysis on α-IC1 and β-IC1′ indicates at least partial occupancy of a p-bonding orbital between C1 and C2. The marked double bond character of the C1−C2 bond hinders rotation about the bond, that is, inhibits interconversion of β-IC1′ and α-IC1. Indeed, the B3LYP/6-31G(d,p) calculated barrier for rotation about the C1−C2 bond in the oxyanion derivative of 1,2-dihydroxypropene (a model for interconversion of a-IC1 and b-IC1′) is 204.3 kJ mol^{-1} (Figure S3, Supporting Information).

However, proton transfer from the now neutral Cys84—SH onto the substrate's C1 center can proceed via β-TS2′ with a barrier of only 82.2 kJ mol^{-1} with respect to β-IC1′. The resulting 2-keto-SRH intermediate complex (IC2) is the same as that formed by reaction of the alternate initial reactant complex α-RC. This is due to the fact that upon protonation of the C1 center via either α-TS2 or β-TS2, the C1−C2 bond formally becomes a single bond, as indicated by its length of 1.54 Å in IC2 (Figure 12). Conversely, the double bond has been localized to the C2═O moiety which now has a length of 1.33 Å in IC2. As a result the intermediate can undergo less hindered rotation about the C1—C2 bond, and thus, both possible initial bound anomers (α-RC and β-RC) can convert to the low lying common intermediate IC2. It is noted that in α-TS2 and β-TS2 the anionic Cys84—S$^-$ thiolate hydrogen bonds with the R-group guanidinium of Arg37. This would help to stabilize Cys84—S$^-$, as has been previously suggested,[9] while also enhancing the acidity of a neutral Cys84—SH.

The PESs for reaction of both α-RC and β-RC via the above water-assisted ring-opening processes to form the common 2-keto-SRH mechanistic intermediate IC2 are overlaid and shown in Figure 13. As can be seen, despite β-RC having a lower barrier for the initial ring-opening reaction step, it is in fact higher than obtained for α-RC due to the higher relative energy of β-RC. Specifically, relative to α-RC, β-TS1′ lies 20.3 kJ mol^{-1} higher in energy than α-TS1′ (Figure 13). Importantly, however, for both α- and β-RC, this initial ring-opening reaction is now enzymatically feasible with barriers of 87.8 and 108.1 kJ mol^{-1}, respectively, relative to α-RC.[34,35] Furthermore, this step represents the highest energy barriers for both systems relative to α- or β-RC encountered along the pathway to formation of the IC2.

The resulting 2-oxyanion intermediates formed, α-IC1 and β-IC1′, both lie significantly lower in energy than α-RC with β-IC1′ being 18.8 kJ mol^{-1} lower in energy than α-IC1. The subsequent barriers for formation of the 2-keto-SRH intermediate via α-TS2 (−28.4 kJ mol^{-1}) and β-TS2′ (−86.1 kJ mol^{-1}) both lie *lower* in relative energy than α- and β-RC, respectively. However, for both anomers, the barriers for this reaction step are distinctly higher than for the preceding reaction step via α-TS1 and β-TS1. This suggests that for both α-SRH (i.e., α-RC) and β-SRH (i.e., β-RC) formation of the 2-

dx.doi.org/10.1021/jp3049907 | J. Phys. Chem. B 2012, 116, 8916−8929

keto-SRH intermediate (IC2) from the preceding 2-oxyanion intermediate (α-IC1 and β-IC1′) is the kinetically limiting step in this initial stage of the overall reaction.[35]

4. CONCLUSIONS

For *S*-ribosylhomocysteinase (LuxS), docking and molecular dynamics (MD) simulations and ONIOM QM/MM methods have been synergistically applied to investigate binding of the *S*-ribosylhomocysteine (SRH) substrate and possible catalytic pathways for formation of a putative linear 2-keto-SRH mechanistic intermediate.

The docking and MD simulations showed that both the α- and β-furanose containing substrates could bind within the active site of LuxS to the Fe(II) ion via their ribose's O2 and O3 oxygens. Furthermore, in both cases, a H_2O was also consistently positioned beneath the ribose ring. The main difference in binding of these anomers results from the different positions of the C1−O1H group. In the β-anomer, it is hydrogen bonded to the R-group carboxylate of an aspartyl residue (Asp37) via a bridging water, while in the alternate α-anomer it instead hydrogen bonds with the R-group imidazole of His11. An alternative linear aldose-containing SRH substrate was shown to also be able to bind within the active site, again, ligating to the Fe(II) via its ribose O2 and O3 oxygens.

Four possible active-site-bound substrate complexes were then optimized using an ONIOM QM/MM approach. Specifically, structures were obtained of the active-site-bound β- (β-RC) and α-furanose (α-RC) containing SRH complexes. In addition, the active-site-bound linear aldose containing SRH complexes β-RC′ and α-RC′, which can be considered as arising from ring-opening of β- and α-RC, respectively, were obtained. These latter complexes were previously experimentally proposed to be the substrate configuration upon which the enzyme acts.[22] Importantly, however, the energetically preferred bound-substrate complex was calculated to in fact be α-RC with β-RC lying 47.5 kJ mol^{-1} higher in energy. Notably, the bound-aldose containing SRH complexes α-RC′ and β-RC′ lie even higher in energy than α-RC by 50.4 and 107.4 kJ mol^{-1}, respectively.

Significantly, the barriers for interconversion of β-RC with β-RC′ and α-RC with α-RC′ were calculated to occur via four-membered ring transition structures with relative energies of 155.6 and 207.6 kJ mol^{-1}, respectively. Due to their very high barriers, these processes are concluded to be enzymatically unfeasible.

However, an alternate mechanism for both β- and α-RC is elucidated in which an active site H_2O facilitates proton transfer from the ribose's Fe(II)-ligated −O2H group onto its ring oxygen O4. This occurs with concomitant abstraction of the −C2H− proton by the thiolate of Cys84 and results in opening of the furanose ring with formation of the $-O2^-$ oxyanion-containing intermediates β-IC1′ and α-IC1, respectively. Importantly, the relative energy barriers for this ring-opening process are now only 60.6 (β-RC to β-IC1′) and 87.8 (α-RC to α-IC1) kJ mol^{-1} with respect to β- and α-RC, respectively, and consequently, are now enzymatically feasible. Notably, both β-IC1′ and α-IC1 are then able to undergo proton transfer from the now neutral Cys84−SH onto C1 with barriers of 82.2 (β-TS2′) and 121.1 (α-TS2) kJ mol^{-1}, respectively. Both processes lead to formation of a common mechanistic 2-keto-SRH intermediate (IC2), which lies significantly lower in energy than α-RC by 251.2 kJ mol^{-1}.

That is, LuxS is able to bind all three possible configurations of the SRH substrate, i.e., containing either an α- or β-furanose ring, the predominate forms in solution, or the linear aldose, with the former α-anomer preferred. The presence of the active site H_2O, however, enables LuxS to be able to act upon any of these three possibilities and catalyze their subsequent reaction to form the common mechanistic intermediate 2-keto-SRH.

■ ASSOCIATED CONTENT

Ⓢ Supporting Information

MD annealing protocol and Cartesian coordinates of the optimized structures reported in this manuscript. This material is available free of charge via the Internet at http://pubs.acs.org.

■ AUTHOR INFORMATION

Corresponding Author

*E-mail: gauld@uwindsor.ca.

Notes

The authors declare no competing financial interest.

■ ACKNOWLEDGMENTS

We thank the Natural Sciences and Engineering Research Council of Canada (NSERC) for funding, SHARCNET for a Graduate Student Fellowship (W.-J. H.) and additional computational resources, and Eric A. C. Bushnell for helpful discussions.

■ REFERENCES

(1) World Health Organization "*Global tuberculosis control: WHO Report 2011*", 2011.
(2) Davies, D. *Nat. Rev. Drug Discovery* **2003**, *2*, 114.
(3) Xavier, K. B.; Bassler, B. L. *Curr. Opin. Microbiol.* **2003**, *6*, 191.
(4) Federle, M. J.; Bassler, B. L. *J. Clin. Invest.* **2003**, *112*, 1291.
(5) Chen, X.; Schauder, S.; Potier, N.; Van Dorsselaer, A.; Pelczer, I.; Bassler, B. L.; Hughson, F. M. *Nature* **2002**, *415*, 545.
(6) Schauder, S.; Shokat, K.; Surette, M. G.; Bassler, B. L. *Mol. Microbiol.* **2001**, *41*, 463.
(7) Miller, M. B.; Bassler, B. L. *Annu. Rev. Microbiol.* **2001**, *55*, 165.
(8) Geske, G. D.; Wezeman, R. J.; Siegel, A. P.; Blackwell, H. E. *J. Am. Chem. Soc.* **2005**, *127*, 12762.
(9) Zhu, J.; Knottenbelt, S.; Kirk, M. L.; Pei, D. *Biochemistry* **2006**, *45*, 12195.
(10) Lewis, H. A.; Furlong, E. B.; Laubert, B.; Eroshkina, G. A.; Batiyenko, Y.; Adams, J. M.; Bergseid, M. G.; Marsh, C. D.; Peat, T. S.; Sanderson, W. E.; Sauder, J. M. l.; Buchanan, S. G. *Structure (London, U.K.)* **2001**, *9*, 527.
(11) Amara, N.; Mashiach, R.; Amar, D.; Krief, P.; Spieser, S. A. H.; Bottomley, M. J.; Aharoni, A.; Meijler, M. M. *J. Am. Chem. Soc.* **2009**, *131*, 10610.
(12) Xu, L.; Li, H.; Vuong, C.; Vadyvaloo, V.; Wang, J.; Yao, Y.; Otto, M.; Gao, Q. *Infect. Immun.* **2006**, *74*, 488.
(13) De Keersmaecker, S. C. J.; Sonck, K.; Vanderleyden, J. *Trends Microbiol.* **2006**, *14*, 114.
(14) Hilgers, M. T.; Ludwig, M. L. *Proc. Natl. Acad. Sci. U.S.A.* **2001**, *98*, 11169.
(15) Rajan, R.; Zhu, J.; Hu, X.; Pei, D.; Bell, C. E. *Biochemistry* **2005**, *44*, 3745.
(16) Zhu, J.; Dizin, E.; Hu, X.; Wavreille, A.-S.; Park, J. K.; Pei, D. *Biochemistry* **2003**, *42*, 4717.
(17) Ruzheinikov, S. N.; Das, S. K.; Sedelnikova, S. E.; Hartley, A.; Foster, S. J.; Horsburgh, M. J.; Cox, A. G.; McCleod, C. W.; Mekhalfia, A.; Blackburn, G. M.; Rice, D. W.; Baker, P. J. *J. Mol. Biol.* **2001**, *313*, 111.
(18) Zhu, J.; Hu, X.; Dizin, E.; Pei, D. *J. Am. Chem. Soc.* **2003**, *125*, 13379.

(19) Gopishetty, B.; Zhu, J.; Rajan, R.; Sobczak, A. J.; Wnuk, S. F.; Bell, C. E.; Pei, D. *J. Am. Chem. Soc.* **2009**, *131*, 1243.
(20) Zhu, J.; Patel, R.; Pei, D. *Biochemistry* **2004**, *43*, 10166.
(21) Voet, D.; Voet, G. J. *Biochemistry*, 4th ed.; John Wiley & Sons, Inc.: New York, 2011.
(22) Pei, D.; Zhu, J. *Curr. Opin. Chem. Biol.* **2004**, *8*, 492.
(23) MOE. 2009.10 ed.; Chemical Computing Group Inc.: Montreal, QC, Canada, 2007.
(24) Bushnell, E. A. C.; Erdtman, E.; Llano, J.; Eriksson, L. A.; Gauld, J. W. *J. Comput. Chem.* **2011**, *32*, 822.
(25) Cornell, W. D.; Cieplak, P.; Bayly, C. I.; Gould, I. R.; Merz, K. M.; Ferguson, D. M.; Spellmeyer, D. C.; Fox, T.; Caldwell, J. W.; Kollman, P. A. *J. Am. Chem. Soc.* **1995**, *117*, 5179.
(26) Frisch, M. J.; Trucks, G. W.; Schlegel, H. B.; Scuseria, G. E.; Robb, M. A.; Cheeseman, J. R.; Scalmani, G.; Barone, V.; Mennucci, B.; Petersson, G. A.; Nakatsuji, H.; Caricato, M.; Li, X.; Hratchian, H. P.; Izmaylov, A. F.; Bloino, J.; Zheng, G.; Sonnenberg, J. L.; Hada, M.; Ehara, M.; Toyota, K.; Fukuda, R.; Hasegawa, J.; Ishida, M.; Nakajima, T.; Honda, Y.; Kitao, O.; Nakai, H.; Vreven, T.; Montgomery, J. A., Jr.; Peralta, J. E.; Ogliaro, F.; Bearpark, M.; Heyd, J. J.; Brothers, E.; Kudin, K. N.; Staroverov, V. N.; Kobayashi, R.; Normand, J.; Raghavachari, K.; Rendell, A.; Burant, J. C.; Iyengar, S. S.; Tomasi, J.; Cossi, M.; Rega, N.; Millam, J. M.; Klene, M.; Knox, J. E.; Cross, J. B.; Bakken, V.; Adamo, C.; Jaramillo, J.; Gomperts, R.; Stratmann, R. E.; Yazyev, O.; Austin, A. J.; Cammi, R.; Pomelli, C.; Ochterski, J. W.; Martin, R. L.; Morokuma, K.; Zakrzewski, V. G.; Voth, G. A.; Salvador, P.; Dannenberg, J. J.; Dapprich, S.; Daniels, A. D.; Farkas, O.; Foresman, J. B.; Ortiz, J. V.; Cioslowski, J.; Fox, D. J. *Gaussian 09*, revision B.01; Gaussian, Inc.: Wallingford, CT, 2009.
(27) Becke, A. D. *J. Chem. Phys.* **1993**, *98*, 1372.
(28) Becke, A. D. *J. Chem. Phys.* **1993**, *98*, 5648.
(29) Lee, C.; Yang, W.; Parr, R. G. *Phys. Rev. B* **1988**, *37*, 785.
(30) Siegbahn, P. E. M.; Blomberg, M. R. A. *Chem. Rev.* **2000**, *100*, 421.
(31) Himo, F. *Theor. Chem. Acc.* **2006**, *116*, 232.
(32) Siegbahn, P. E. M.; Borowski, T. *Acc. Chem. Res.* **2006**, *39*, 729.
(33) Calculated at the B3LYP/6-31G(d,p) level of theory.
(34) Llano, J.; Gauld, J. W. Mechanistics of Enzyme Catalysis: From Small to Large Active-Site Models. In *Quantum Biochemistry*; Matta, C. F., Ed.; Wiley-VCH Verlag GmbH & Co. KGaA: Weinheim, Germany, 2010; Vol. 2.
(35) Laidler, K. J. *Chemical Kinetics*, 3rd ed.; HarperCollins Publishers, Inc.: New York, 1987.